# Photoelectron Spectroscopy of Biacetyl and Its Cluster Anions

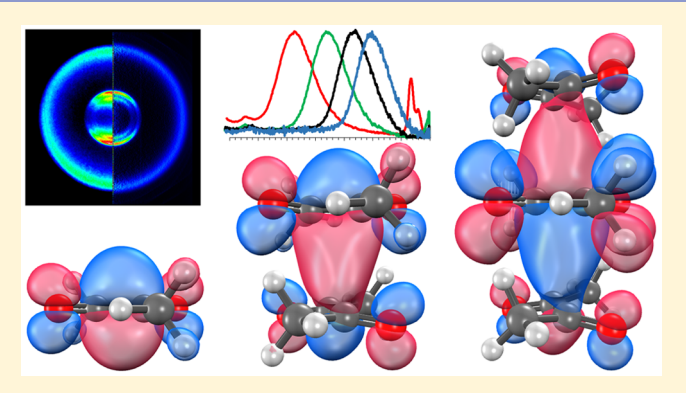
Published as part of The Journal of Physical Chemistry virtual special issue "Hanna Reisler Festschrift".

Yerbolat Dauletyarov, Adam A. Wallace, Christopher C. Blackstone, and Andrei Sanov\*

Department of Chemistry and Biochemistry, The University of Arizona, Tucson, Arizona 85721, United States

Supporting Information

ABSTRACT: Photoelectron spectroscopy of the biacetyl (dimethylglyoxal) anion reveals the properties of the ground singlet and lowest triplet electronic states of the neutral biacetyl (BA) molecule. Due to the broad and congested nature of the singlet transition, which peaks at a vertical detachment energy VDE = 1.12(5) eV, only an upper bound of the adiabatic electron affinity of BA could be determined: EA(BA) < 0.7 eV. A narrower and more structured triplet band peaking at VDE = 3.17(2) eV reveals the adiabatic electron binding energy of the triplet to be 3.05(2) eV. These results are in good agreement with ab initio (coupled-cluster) calculations. The lowest-energy structures of the anion, singlet, and triplet states of biacetyl are characterized by



different orientations of the methyl groups within the molecular frame. In the ground singlet state of neutral BA, the methyl torsion is offset by  $\sim 60^{\circ}$  compared to that of the anion, while in the triplet the methyl orientation is similar to that of the anion. Photoelectron spectra of the cluster anions reveal that the intermolecular interactions in the homogeneously solvated (BA), clusters are significantly stronger than the interactions of BA with N2O or even of BA with H2O. To account for these observations,  $\pi - \pi$  bonded structures of the dimer and trimer anions of biacetyl are proposed based on density-functional theory calculations. The analysis of the proposed structures indicates that the negative charge in the  $(BA)_n^-$  cluster anions, at least in the dimer and the trimer, is significantly delocalized between all BA moieties present and there is a significant degree of covalent bonding within the cluster.

# 1. INTRODUCTION

Biacetyl (BA) is the common name of dimethylglyoxal. Together with singly substituted methylglyoxal (MG) and unsubstituted glyoxal, BA is a member of the family of small dicarbonyls with important roles in atmospheric chemistry (see Scheme 1).1-3 It is a volatile organic compound, relatively

# Scheme 1

abundant in the atmosphere. Its oxidation in the presence of nitric oxide leads to the formation of ozone and other important processes.4

In this report, we investigate the structure and spectroscopy, along with electron attachment and cluster formation properties of biacetyl. This work builds on our previous studies of glyoxal<sup>5</sup> and methylglyoxal.<sup>6</sup> Surprisingly little is known about this relatively simple yet important molecule, especially concerning its photochemistry, oligomerization (cluster formation), and interactions with electrons and ions. The

adiabatic electron affinity of BA was determined previously to be 0.69(1) eV using an indirect temperature dependent equilibrium ion/molecule reaction method.<sup>7</sup> The electron binding and other properties of BA oligomers, however, have remained largely unknown. The most recent study of BA oligomers was the 1938 work by Molds and Riley8 investigating the polymerization of MG and BA. They reported that MG undergoes polymerization with mass loss, and the rate of the process increases with the addition of water, while BA was not found to polymerize under the same conditions.

The present study of BA cluster anions represents the first spectroscopic investigation of biacetyl oligomerization in anionic environments. We report the photoelectron spectra of BA and its clusters measured by means of anion photoelectron imaging. Transitions from the anion to the lowest singlet and triplet states of neutral BA are identified, and their properties are discussed in relation to the distinct geometric structures of the BA anion, the ground-state BA singlet, and the lowest triplet. In addition, we discuss the energetics and structural properties of small clusters of biacetyl,

Received: February 8, 2019 Revised: April 15, 2019 Published: April 24, 2019

focusing in particular on the homogeneous (BA)<sub>n</sub><sup>-</sup> cluster anions. We show that the interactions between the monomer moieties in these clusters are stronger than anionic hydrogen bonding between the BA<sup>-</sup> anion and a water molecule, indicating charge delocalization and significant covalent character of the interactions between the monomer groups.

# 2. EXPERIMENTAL METHODS

The experiments were carried out using a negative-ion photoelectron<sup>9</sup> imaging<sup>10–12</sup> spectrometer described elsewhere. 13 In short, 99% pure biacetyl (Alfa Aesar, Thermo Fisher Scientific) was placed in a sample holder connected to the gas delivery lines and the pulsed nozzle located inside the ion source chamber. By passing the N2O carrier gas at an absolute backing pressure of approximately 2.7 atm over the liquid sample, the BA vapor (vapor pressure 0.075 atm at room temperature) was delivered to the source chamber. The resulting ~3% mixture of BA vapor in N<sub>2</sub>O was expanded into the high-vacuum chamber (10<sup>-7</sup> Torr base, 10<sup>-5</sup> Torr operational pressure) through a pulsed supersonic nozzle (General Valve Series 9, Parker, Inc.) operating at a 50 Hz repetition rate matching that of the laser. The supersonic expansion was bombarded with ~200 eV electrons from an electron cannon leading to the formation of anions via slow secondary electron attachment. The electron "cannon" is a simplified device constructed from a conventional custom-built electron gun<sup>13</sup> by stripping it off the horizontal and vertical electron deflectors and the Einzel lens and placing a grounded metal plate with a 3.5 mm diameter aperture in front of the electron-emission assembly consisting of a floated thoriumcoated iridium ribbon filament and an anode plate.

The anions and cluster anions were extracted into a Wiley–McLaren<sup>14</sup> linear time-of-flight mass-spectrometer using a repeller plate pulsed from the ground potential to approximately –900 V at the approximate time of the arrival of the ions carried by the supersonic expansion.<sup>15</sup> The anions were then further accelerated to approximately 2.5 keV of kinetic energy and separated according to their mass-to-charge ratios within a 2-m long flight tube before entering the detection region of the instrument, housing a velocity-map<sup>16</sup> imaging assembly.

Within the imaging assembly, the anion beam was intersected at 90° with a pulsed (7 ns) linearly polarized laser beam from a 50 Hz Spectra Physics LAB-130-50 Nd:YAG laser. The experiments described here used 532 and 355 nm radiation obtained as the second and third harmonics of the laser's 1064 nm fundamental output. The electrons photodetached from the anions were electrostatically projected by a series of velocity-map electrodes in the direction orthogonal to both the ion and laser beams and detected by a 40 mm diameter position-sensitive dual-microchannel-plate detector coupled to a P43 phosphor screen (Burle, Inc.). Photoelectron impact positions on the detector were recorded by a thermoelectrically cooled CCD camera (CoolSNAP Myo, Photometrics, Inc.). Raw images were typically collected for  $\sim 10^6$  experimental cycles and reconstructed using the inverse Abel transformation<sup>12</sup> implemented in the BASEX program.<sup>17</sup> The resulting radial distributions were converted to photoelectron spectra using an energy scale calibrated based on the well-known electron affinity of atomic oxygen. 18,19

# 3. EXPERIMENTAL RESULTS AND ANALYSIS

**3.1. The Anion of Biacetyl.** A sample 355 nm photoelectron image and the corresponding photoelectron spectrum of biacetyl anion (BA<sup>-</sup>) are presented in Figure 1. For

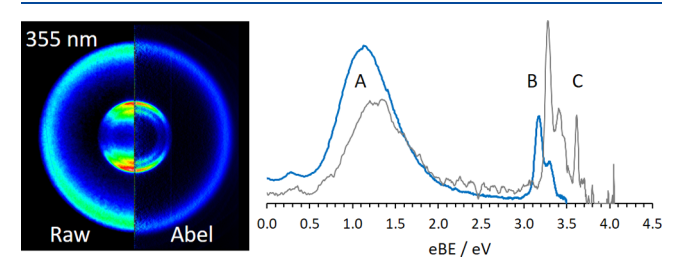


**Figure 1.** Left: a composite photoelectron image of BA<sup>-</sup> obtained at 355 nm. The direction of the laser polarization is vertical in the image plane. The left half of the composite image represents the corresponding half of the raw experimental image, while the right half represents the corresponding Abel inversion. The corresponding photoelectron spectrum is shown to the right of the image (bold blue curve). It is compared to the previously reported (ref 6) photoelectron spectrum of methylglyoxal obtained at 306 nm (gray curve).

comparison, the previously published<sup>6</sup> spectrum of methylglyoxal anion (MG<sup>-</sup>) obtained at 306 nm is reproduced in the figure (gray line). These and all other spectra in this work are plotted versus electron binding energy (eBE), defined as eBE = hv - eKE, with hv being the photon energy and eKE being the electron kinetic energy. The BA<sup>-</sup> and MG<sup>-</sup> spectra have similar profiles, although all bands in the MG<sup>-</sup> spectrum are shifted somewhat to higher binding energies compared to the BA<sup>-</sup> bands. Two bands, labeled A and B, are observed in both the BA<sup>-</sup> and MG<sup>-</sup> spectra. For MG<sup>-</sup>, an additional band labeled C is present. A similar band is expected to appear in BA<sup>-</sup> spectra at shorter (compared to 355 nm) wavelengths.

The bands observed in the MG<sup>-</sup> spectrum were previously assigned to the corresponding transitions and low-lying electronic states of neutral MG.<sup>6</sup> Similarly, in the BA<sup>-</sup> spectrum, band A is assigned to the transition from the ground state of the anion to the singlet ground state of neutral BA, while band B is assigned to the transition from the anion to the lowest triplet state of BA. Bands A in the BA<sup>-</sup> and MG<sup>-</sup> spectra are broad and congested, indicative of significant geometry differences between the anion and the respective neutral equilibria, while bands B are more structured and narrow in both cases. The position of band A's maximum corresponds to the anion's vertical detachment energy (VDE), while its poorly defined onset corresponds to the adiabatic electron affinity of the neutral molecule.

From the BA $^-$  spectrum in Figure 1, the VDE of BA $^-$ , corresponding to detachment to the singlet state of the neutral, is determined to be 1.12(5) eV, while the EA of BA is estimated to be <0.7 eV. The weak signals appearing slightly above the baseline at eBE  $\sim$  0.3 eV in both the BA $^-$  and MG $^-$  spectra in Figure 1 are artifacts attributed to the imaging detector's edge effects and were disregarded in the analysis. The above determination of the upper bound of electron affinity is consistent with the previous determination of this property, 0.69(1) eV, using the temperature-dependent equilibrium ion—molecule reaction method.  $^7$ 

The BA<sup>-</sup> spectrum in Figure 1 also reveals the properties of the lowest triplet state of BA. Based on the analysis of band B, the VDE of BA<sup>-</sup> corresponding to detachment to the triplet is

Table 1. Vertical and Adiabatic Energies (in eV) of the Singlet  $(X^1A_g)$  and Triplet  $(a^3A_u)$  Electronic States of Biacetyl Relative to the BA<sup>-</sup> Anion  $(X^2A_u)$  Equilibrium

	singlet $(X {}^{1}A_{g})$		triplet $(a^{3}A_{u})$	
method <sup>a</sup>	vertical (VDE)	adiabatic (EA)	vertical (VDE)	adiabatic (EA)
M06-2X <sup>b</sup>	1.379	0.802	3.410	3.268
$CCSD^b$	1.092	0.545	3.369	3.248
EOM-IP- CCSD <sup>c</sup>	1.037		3.114	
experiment	1.12(5)	< 0.7	3.17(2)	3.05(5)

"All calculations used the aug-cc-pVDZ basis set. "The relative state energies were obtained by subtracting the anion energy from the corresponding (vertical or adiabatic, as appropriate) neutral state energy. "The single-point EOM-IP calculations employed the doublet ( $^2A_u$ ) anion reference and were carried out for the CCSD/aug-cc-pVDZ optimized geometry of the anion. The vertical singlet-state excitation energy was calculated by considering the lowest-energy alpha-spin electron-removal transition of  $A_u$  symmetry ( $^2A_u \rightarrow ^1A_g$ ), while the triplet-state energy was calculated using the corresponding beta-spin transition of  $A_v$  symmetry ( $^2A_u \rightarrow ^3A_u$ ).

3.17(2) eV, while the corresponding EA (adiabatic binding energy), determined based on band B's onset, is 3.05(5) eV. These experimentally determined VDE and EA values are included in Table 1.

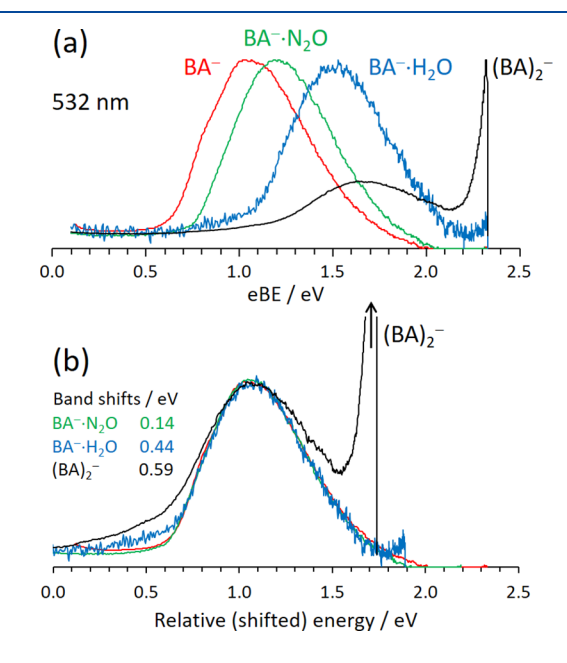
**3.2. Cluster Anions of Biacetyl.** Figure 2(a) shows 532 nm photoelectron spectra of BA<sup>-</sup>, its heterogeneously solvated clusters BA<sup>-</sup>·N<sub>2</sub>O and BA<sup>-</sup>·H<sub>2</sub>O, and the (BA)<sub>2</sub><sup>-</sup> dimer anion. As expected, based on the 355 nm spectrum in Figure 1, the 532 nm BA<sup>-</sup> spectrum consists of a single broad band (defined as band A in Figure 1). The BA<sup>-</sup>·N<sub>2</sub>O and BA<sup>-</sup>·H<sub>2</sub>O spectra are both similar to the unsolvated BA<sup>-</sup> spectrum but shifted to larger eBEs by 0.14(1) eV and 0.44(1) eV, respectively, as determined below. These shifts are consistent with the solvation stabilization energies expected for the addition of one N<sub>2</sub>O or one H<sub>2</sub>O molecule to the anion.

The  $(BA)_2^-$  dimer anion spectrum, on the other hand, consists of two transitions: a broad band, similar to the bands observed in the BA<sup>-</sup>, BA<sup>-</sup>·N<sub>2</sub>O, and BA<sup>-</sup>·H<sub>2</sub>O spectra, plus an intense, relatively sharp peak in the vicinity of the photon energy spectral cutoff (low-eKE electrons). The broad  $(BA)_2^-$  band shows a significant shift relative to the BA<sup>-</sup> spectrum. The magnitude of this shift is larger than that induced by the addition of H<sub>2</sub>O to BA<sup>-</sup>, suggesting that the interaction between the two BA moieties in  $(BA)_2^-$  is stronger than the anionic hydrogen bonding between BA<sup>-</sup> and H<sub>2</sub>O. Since (unlike H<sub>2</sub>O) BA has no dipole moment, the magnitude of the  $(BA)_2^-$  band shift can hardly be attributed to mere electrostatic forces within a BA<sup>-</sup>·BA ion-molecule complex. Therefore, the interaction between the two BA moieties in  $(BA)_2^-$  is likely to have some covalent character.

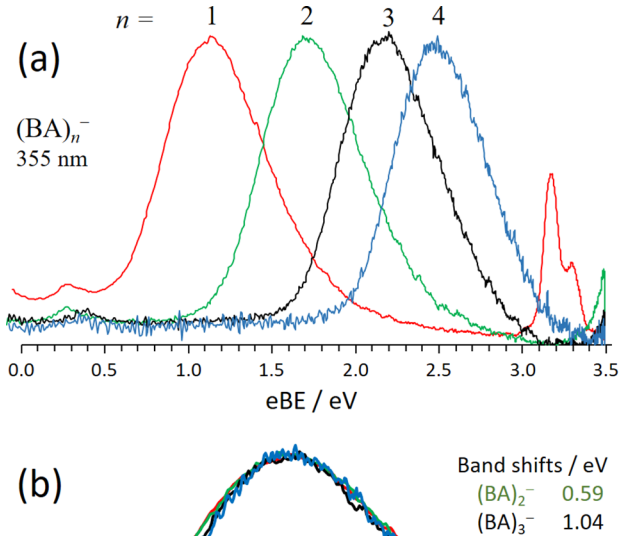
To quantify the observed band shifts, we fit the broad bands in each of the  $BA^-\cdot N_2O$ ,  $BA^-\cdot H_2O$ , and  $(BA)_2^-$  spectra to the unsolvated  $BA^-$  spectrum, treating the band shift as an adjustable parameter. Figure 2(b) shows the three cluster spectra from (a), each shifted back in energy to overlap with the unsolvated  $BA^-$  band (the relative intensities were also scaled as necessary). This procedure yielded the following determinations of the observed band shifts in the  $BA^-\cdot N_2O$ ,  $BA^-\cdot H_2O$ , and  $(BA)_2^-$  spectra relative to  $BA^-$ : 0.14(1) eV, 0.44(1) eV, and 0.59(1) eV, respectively. These values (without the error bars) are included in Figure 2(b).

To investigate the character of the interactions between BA moieties in cluster environments, we collected additional data of the BA dimer, trimer, and tetramer anions. The motivation for considering not only the dimer but also the larger clusters is rooted in the properties of other strongly bound dimer anions. Often, if a particular compound forms a covalently bound dimer anion, this anion becomes the "core" of the larger homogeneously solvated clusters. That is, if two molecular moieties X exhibit a strong (covalent) interaction upon the attachment of an electron, this interaction will result in a significant photoelectron band shift for  $X_2^-$  compared to  $X^-$ . If the shift is larger than expected for electrostatic ion-molecule interactions, the dimer anion structure is more appropriately described as  $X^{-1/2} \cdot X^{-1/2}$  or  $X_2^-$ , with the charge shared between the two X moieties, rather than X-X. The addition of more X moieties to the dimer anion core leads to additional stabilization of the  $X_n^-$  clusters, but the sequential band shifts observed for n = 3 and larger clusters will be significantly smaller than for n = 2 relative to n = 1. This is because the third and other additional X moieties play the role of (neutral) solvent molecules, stabilizing the cluster by means of electrostatic solvation interactions with the anionic cluster core. These ion-neutral interactions are weaker than the covalent interaction bonding the first two X moieties together within the  $X_2^-$  core anion, and the larger  $X_n^-$  clusters are therefore more appropriately described as  $X_2 \cdot X_{n-2}$ . Wellknown examples of such behavior are found in the previous studies of the CO<sub>2</sub>, OCS, CS<sub>2</sub>, and oxygen cluster anions.<sup>20–26</sup>

Figure 3(a) displays the BA<sup>-</sup>,  $(BA)_2^-$ ,  $(BA)_3^-$ , and  $(BA)_4^-$  photoelectron spectra obtained at 355 nm (the BA<sup>-</sup> spectrum is reproduced from Figure 1). The respective band maxima are at 1.12(5) eV, 1.71(5) eV, 2.16(5) eV, and 2.46(5) eV. The corresponding spectral shifts relative to the monomer anion are 0.59(1) eV for the dimer, 1.04(1) eV for the trimer, and 1.34(1) eV for the tetramer. The corresponding sequential



**Figure 2.** (a) Photoelectron spectra of BA $^-$  and its solvated clusters BA $^-$ N<sub>2</sub>O and BA $^-$ H<sub>2</sub>O, as well as the (BA)<sub>2</sub> $^-$  dimer anion, obtained at 532 nm. (b) The same spectra as in (a) shifted back in energy for the best overlap with the BA $^-$  spectrum. The shifts are indicated in the figure. Their estimated uncertainty is  $\pm 0.01$  eV.



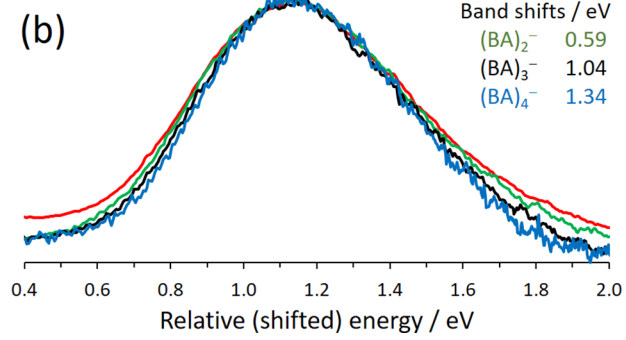


Figure 3. (a) Photoelectron spectra of  $(BA)_n$ , n = 1-4 obtained at 355 nm. (b) The same spectra as in (a) shifted back in energy for the best overlap with the BA spectrum. The band shifts are indicated in the figure. Their estimated uncertainty is  $\pm 0.01$  eV.

shifts (relative to the preceding member of the series rather than BA<sup>-</sup>) are 0.59(1) eV from the monomer to the dimer, 0.45(1) eV from the dimer to the trimer, and 0.30(1) eV from the trimer to the tetramer. The shift values were determined using the same procedure as above: by fitting the entire (BA), (n > 1) bands, shifted back in binding energy, to the BA<sup>-</sup> band and treating the magnitude of the shift as an adjustable parameter. This procedure results in band shift errors that are smaller than those for the absolute band positions. The overlapped (shifted) spectra from Figure 3(a) are shown in Figure 3(b), and all shift values are summarized in Table 2.

None of the  $(BA)_n^-$  spectra in Figure 3(a) include the sharp intense bands at eBE  $\sim 2.3$  eV, similar to the one observed in the 532 nm (BA)<sub>2</sub> spectrum in Figure 2(a). Instead, each of the 355 nm cluster anion spectra shows similarly shaped but much weaker bands appearing at eBE ~ 3.5 eV, i.e. also at the photon-energy spectral cutoff, just like the sharp band in the 532 nm (BA)<sub>2</sub> spectrum. Hence, these slow-electron bands cannot be due to direct photodetachment to any specific state of the neutral species, as such transition would appear at the same eBE, independent of the wavelength. These slow-electron bands are likely signatures of autodetachment from excited states of the cluster anions. That their intensity varies with wavelength is consistent with this interpretation. It is plausible that the excited  $(BA)_2^-$  state involved is in (near-) resonance with 532 nm photons, resulting in the intense autodetachment signal in the (BA)<sub>2</sub> spectrum in Figure 2(a). The 355 nm photons may be accessing the higher-energy wing of this transition, resulting in much weaker autodetachment signatures in the  $(BA)_n$ ,  $n \ge 2$ , spectra in Figure 3(a). Finally, the observation of the autodetachment peaks for  $(BA)_n^-$ ,  $n \ge 2$ ,

Table 2. Vertical Detachment Energies, Band Shifts, and Cluster Solvation Energies (All in eV), Calculated Using the M06-2X/aug-cc-pVDZ Method for the (BA), Cluster **Anions** 

	BA <sup>-</sup>	$(BA)_2^-$	$(BA)_3^-$	$(BA)_2^-$
Sovation energy (DFT) <sup>a</sup>	0	0.952	1.670	_b
VDE				
$\mathrm{DFT}^c$	1.379 <sup>d</sup>	1.947	2.512	_
$(CCSD+DFT)^e$	1.092	1.661	2.226	_
Experiment <sup>f</sup>	1.12(5)	1.71(5)	2.16(5)	2.46(5)
$\Delta VDE (DFT)$				
Relative to BA <sup>-g</sup>	n/a	0.569	1.134	_
Sequential <sup>h</sup>	n/a	0.569	0.565	_
Band shift (experiment) <sup>i</sup>				
Relative to BA <sup>-g</sup>	n/a	0.59(1)	1.04(1)	1.34(1)
Sequential <sup>h</sup>	n/a	0.59(1)	0.45(1)	0.30(1)

<sup>a</sup>Solvation energies for the  $(BA)_n^-$  cluster anions (up to n=3 only) were calculated as  $E_{\text{soly}}(n) = E[BA^-] + (n-1)E[BA] - E[(BA)_n^-]$ . The energies of all species were calculated for the corresponding optimized ground-state structures: the  $C_{2h}$  (an) and  $C_{2h}$  (nu) geometries of BA and BA, respectively (as defined in Figure 4), and the  $C_2$  (an-nu) geometry of the dimer anion (shown in Figure 5). <sup>b</sup>Dashes indicate that the corresponding property was not calculated for the given species; n/a indicates that the property is not applicable to this species. <sup>c</sup>The vertical detachment energy (VDE) for each ion is calculated as the difference between the neutral and anion energies, both determined at the optimized geometry of the anion. <sup>d</sup>For comparison, the VDE values for BA calculated at the CCSD and EOM-IP-CCSD levels of theory are 1.092 and 1.037 eV, as summarized in Table 1. These results are in much better agreement with the experiment, compared to the DFT value. eThe VDE (CCSD +DFT) values were determined by adding the VDE = 1.092 eV of BA determined using the CCSD method (see footnote e) to the corresponding (BA)<sub>n</sub> band shifts (relative to BA<sup>-</sup>), determined using the M06-2X DFT method, also included in this table. From the data in Figure 3(a).  ${}^g\Delta VDE$  (DFT) for a particular (BA) $_n^-$  cluster is determined as the difference between this cluster's VDE and that of BA<sup>-</sup>:  $\Delta$ VDE(n) = VDE(n) - VDE(1).  $^h$ Same as above but relative to the preceding member of the series:  $\Delta VDE(n) = VDE(n) - VDE(n-1)$ 1). From the fits in Figure 3(b).

but not for the unsolvated BA anion, strongly suggests that the excited anionic state responsible for the autodetachment involves electronic excitation that is intermolecular in character. This excitation does not occur in an isolated BAanion, because it requires electron delocalization between at least two BA moieties. This observation supports the hypothesis that the intermolecular interactions within the  $(BA)_n^-$ ,  $n \ge 2$ , cluster anions are partially covalent in character.

### 4. DISCUSSION

To assist in interpretation of the results, we performed theoretical calculations for the various anion, neutral, and cluster anion species studied in this work. All calculations were performed using the QChem 5.1 software package.

First, the geometric structures and relative energies of BA<sup>-</sup> and the corresponding neutral molecule in the lowest singlet and triplet states were determined using the coupled cluster method with single and double excitations (CCSD). Second, the BA vertical detachment energies corresponding to transitions to the singlet and triplet states of the neutral were calculated using both the CCSD and the equation-of-motion ionization-potential CCSD (EOM-IP-CCSD) methodologies.<sup>28</sup> Third, the structures, solvation energies, and electron

detachment energetics of the  $(BA)_2^-$  and  $(BA)_3^-$  cluster anions were investigated using density functional theory (DFT), specifically the Minnesota 06 functional (M06-2X).<sup>2</sup> This functional was chosen for its known performance on a delocalized system involving noncovalent interactions (e.g., clusters).<sup>29</sup> All calculations employed Dunning's augmented correlation-consistent basis set of double-ζ quality (aug-ccpVDZ).

4.1. Biacetyl Anion, Singlet, and Triplet: Geometric **Structures.** The equilibrium geometries of biacetyl in its anion, ground-state neutral singlet, and lowest triplet states are shown in Figure 4. The geometric parameters defining these

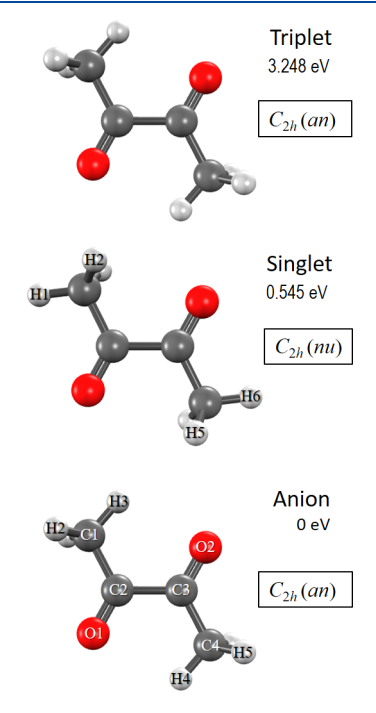


**Figure 4.** Bottom to top in order of increasing energy: BA anion (X  ${}^{2}A_{u}$ ), singlet  $(X {}^{1}A_{g})$ , and triplet  $(a {}^{3}A_{u})$  structures optimized at the CCSD/aug-cc-pVDZ level of theory. The energies shown are adiabatic electronic energies relative to the anion equilibrium. Each of the three structures belongs to the  $C_{2h}$  symmetry point group, and all geometric parameters are given in Table 3. The torsional orientations of the methyl groups in the neutral singlet and anion structures define the respective "neutral" (nu) and "anion" (an) structural motifs. The nu and an designations refer to the geometric structures, not the charges (for example, the neutral triplet state adopts the an structural motif).

structures, optimized at the CCSD level of theory, are summarized in Table 3. All three structures belong to the  $C_{2h}$  symmetry point group, with all heavy atoms located in the same plane.

Similar to methylglyoxal, 6 the apparent distinction between the geometries of biacetyl anion, singlet, and triplet is internal orientation of the methyl groups. Specifically, the anion and the triplet structures are qualitatively similar to each other, with the H3 and H4 hydrogens (see Figure 4) lying in the heavy-atom plane and pointing toward the opposing carbonyl group, while in the singlet state, the methyl groups are internally rotated by about 60°, bringing the H1 and H6 hydrogens, pointing toward the adjacent carbonyls, into the heavy-atom plane. We will use the torsional orientations of the methyl groups in the singlet and anion structures to define the

Table 3. Geometric Parameters for the Three  $C_{2h}$  Symmetry Structures Shown in Figure 4: the BA<sup>-</sup> Anion  $(X^2A_u)$ Electronic State), the BA Ground State Singlet  $(X^{1}A_{\sigma})$ , and the Lowest Triplet  $(a^{3}A_{\mu})^{a}$ 

parameter	anion	singlet	triplet
C2-C3	1.446	1.550	1.489
C1-C2	1.530	1.514	1.519
C2-O1	1.282	1.222	1.249
C1-H1	1.107	1.099	1.103
C1-H3	1.101	1.103	1.102
O1-C2-C3	123.9	119.1	120.8
O1-C2-C1	118.4	124.1	121.6
C2-C1-H1	109.4	109.2	109.5
C2-C1-H3	111.4	109.7	108.2
C3-C2-C1-H1	121.5	180.0	120.5
C3-C2-C1-H3	0.0	58.5	0.0

<sup>a</sup>All structures were optimized at the CCSD theory level using the aug-cc-pVDZ basis set. The numbering of the atoms is defined in Figure 4. The bond lengths are in Angstroms, and the angles are in degrees. Bold emphasis: neutral (singlet and triplet) parameters with the most significant deviations from the anion geometry (at least 0.05 Å or  $4^{\circ}$ ).

respective "neutral" (nu) and "anion" (an) structural motifs. The *nu* and *an* designations refer to molecular geometries, not necessarily the charges. For example, the triplet neutral state of BA adopts the an structural motif. Including the symmetry, we will describe the anion  $(^{2}A_{u})$ , singlet  $(^{1}A_{v})$ , and triplet  $(^{3}A_{u})$ structures shown in Figure 4 as  $C_{2h}$  (an),  $C_{2h}$  (nu), and  $C_{2h}$ (an), respectively.

We have verified that the  $C_{2h}$  (nu) geometry is the true potential minimum of the ground-state singlet BA, while the  $C_{2h}$  (an) structural motif corresponds to the potential minima of the anion and the triplet. Specifically, DFT (M06-2X) calculations showed that the structures in Figure 4 have no imaginary vibrational frequencies. To the contrary, the  $C_{2h}$ (an) geometry (reoptimized subject to the symmetry constraint) has two imaginary frequencies on the singlet potential energy surface and lies 0.086 eV higher than the corresponding  $C_{2h}$  (nu) structure. Thus, while the methyl groups in BA may exhibit nearly free internal rotation, the corresponding torsional potential features three (for three hydrogens) equivalent shallow minima separated by 120°, each corresponding to the  $C_{2h}$  (nu) structure. The opposite is true for the anion and the triplet. Similar DFT calculations revealed no imaginary frequencies for the  $C_{2h}$  (an) anion and triplet structures, while the corresponding  $C_{2h}$  (nu) geometries each indicated two imaginary frequencies and were found to be 0.028 eV (anion) and 0.034 eV (triplet) higher than the respective  $C_{2h}$  (an) structures.

The differences between the anion and neutral equilibrium structures explain the broad nature of the singlet band (band A) in the BA<sup>-</sup> spectra in Figures 1–3. Even though the internal methyl rotation is visually the most striking difference between the anion and neutral equilibrium geometries, the band breadth cannot be predominantly attributed to this degree of freedom. We caution that the singlet band in the unsubstituted glyoxal spectrum,5 which can be viewed in comparison with the methylglyoxal spectrum in ref 6, is nearly as broad in the absence of the methyl groups, as bands A in both the MG<sup>-</sup> and BA spectra presented here in Figure 1. Considering the geometric parameters in Table 3, we note that in addition to

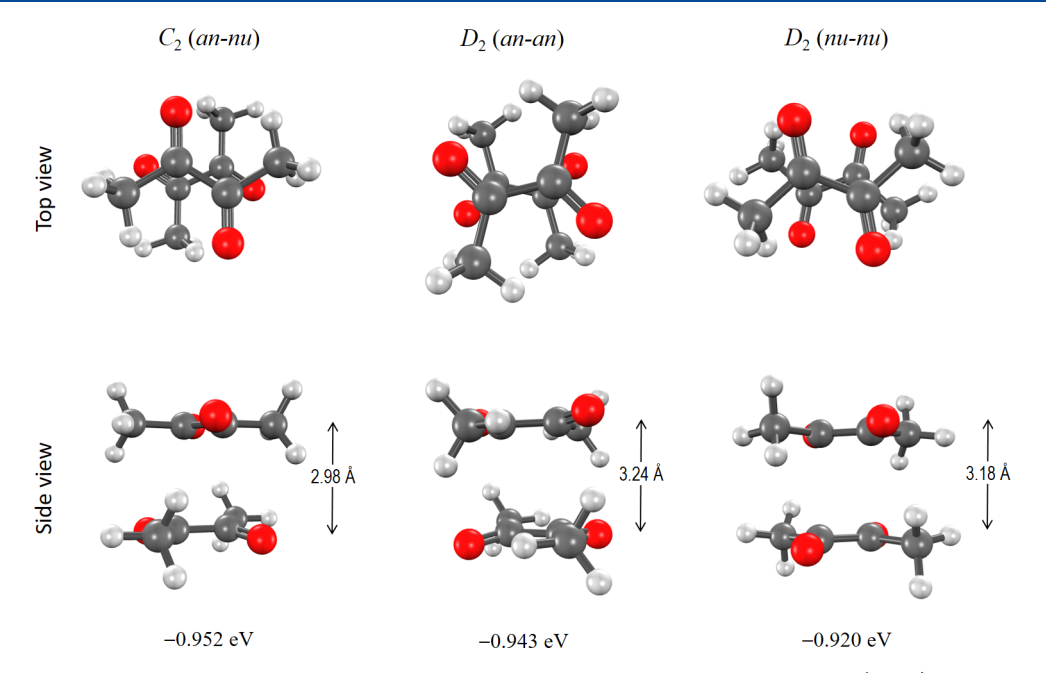


Figure 5.  $(BA)_2^-$  structures optimized at the M06-2X level of theory with the aug-cc-pVDZ basis set. The  $C_2$  (an-nu) structure consists of one BA moiety adopting the "anion" (an) structural motif and one BA moiety adopting the "neutral" (nu) motif (the motifs are defined in Figure 4). In the  $C_2$  (an-nu) structure shown, the an-moiety is in the front of the top view and at the top of the side view. The total Mulliken charges of the an and nu BA moieties in this structure are -0.52 and -0.48, respectively. The  $D_2$  (an-an) and  $D_2$  (nu-nu) structures consist of two equivalent an-BA and two equivalent nu-BA moieties, respectively, each moiety in each case carrying a Mulliken charge of -0.5. The separations between the monomer groups indicated in the figure (side views) are defined as the distance between the centers of the respective C2-C3 bonds (see Figure 4 for atom numbers). Complete dimer anion structures are included in the Supporting Information. The energy of each structure shown is the negative of the cluster solvation energy, defined relative to the adiabatic BA + BA $^-$  dissociation limit (see footnote a in Table 2).

the methyl rotation, there are other significant, if less obvious, differences between the anion and neutral singlet structures, particularly in regard to the central C–C bond and the C=O bonds. Plus, there are significant differences in the angles between the in-plane heavy-atom bonds in the molecule. The geometric parameters that exhibit the most significant changes between the anion and the neutral states are bolded in Table 3, and it is the excitation of all of these bolded degrees of freedom together that gives the width of the singlet band. To the contrary, the geometric differences between the anion and the neutral triplet structures are less significant, consistent with the triplet band (band B) in Figure 1 being considerably narrower and less congested than the singlet band.

**4.2.** Biacetyl: Energetics of the Anion, Singlet, and Triplet States. The calculated vertical and adiabatic energies of the singlet and triplet states of BA relative to the anion equilibrium are summarized in Table 1, where they are compared to the experimental results. The vertical excitation energies of the singlet and the triplet, relative to the anion, correspond to the experimental VDEs, while the adiabatic values correspond to the respective EAs. The energies of the three states were first minimized using DFT (M06-2X) and then reoptimized at the CCSD level of theory. The corresponding structures are shown in Figure 4 and discussed in Section 4.1. The resulting equilibrium energies were used to determine the adiabatic energy gaps. For vertical excitations, the differences between the single-point energies at the equilibrium geometry of the anion were considered.

The VDEs of BA $^-$  corresponding to transitions to both singlet and triplet neutral states were also determined by the EOM-IP-CCSD method using the CCSD-optimized anion geometry. The X  $^2$ A $_u \rightarrow X$   $^1$ A $_g$  photodetachment was modeled

as the lowest-energy  $A_u$  symmetry transition removing an alpha-spin electron from the anion reference, while the  $X^2A_u \rightarrow a^3A_u$  detachment energy was calculated using the corresponding beta-spin transition of  $A_v$  symmetry.

The VDE predicted by the CCSD method for the singlet transition, 1.092 eV, is in excellent agreement with the experimental result, 1.12(5) eV, while DFT overestimates it by  $\sim$ 0.3 eV. This observation will play a role in the discussion of cluster energies and structures in Section 4.3. The EOM-IP-CCSD prediction for the singlet state, 1.037 eV, agrees quite well with the CCSD value and with the experiment. For the triplet transition, however, there is a sizable ( $\sim 0.2$  eV) discrepancy between the CCSD prediction and the experimentally measured VDE. The CCSD result is actually closer to the corresponding DFT prediction than to the experiment, while EOM-IP-CCSD yields a much better agreement for the triplet state: 3.114 eV vs the 3.17(2) experimental value. The superior performance of the EOM method for the triplet state is even more noteworthy, if one considers the vertical singlettriplet excitation energy (at the anion geometry):  $\Delta E_{S-T}$  = 2.077 eV (EOM-IP-CCSD), which is in perfect agreement with the 2.05(5) eV experimental value. In comparison, CCSD overestimates this gap by more than 0.3 eV. As noted by Krylov and others, in calculating excitation energies, it is important to describe the initial and final states in a consistent manner, i.e. using the same reference.<sup>28</sup> While the EOM-IP-CCSD method does just that, the energy gaps in CCSD calculations are calculated as the deltas between the results determined using two different references.

**4.3. Structures of Biacetyl Cluster Anions.** Coupled-cluster calculations become prohibitively expensive for larger systems. We used the M06-2X functional (chosen for its

performance on delocalized systems with noncovalent interactions)<sup>29</sup> to investigate the properties of biacetyl cluster anions. We focused on the structures and energetics of  $(BA)_2^-$  and  $(BA)_3^-$ .

Exploratory geometry optimizations were carried out for the dimer anion, starting from several initial geometries without geometric or symmetry constraints. These explorations led us to identify three plausible  $(BA)_2^-$  structures, which were then optimized under the appropriate symmetry constraints. Vibrational frequency calculations were used to confirm that the proposed dimer-anion structures correspond to potential minima.

The three  $(BA)_2^-$  structures are shown in Figure 5, while complete details are given in the Supporting Information. Each structure is sandwich-like in appearance and is shown in two projections: "top view" and "side view". The separation between the individual BA moieties is  $\sim 3$  Å in each case, as indicated in the figure and defined in the caption. The energies are given relative to isolated  $BA^- + BA$  (at their respective equilibria), determined using the same method. The three structures are all close in energy, and the most apparent geometric difference between them is the *intra*molecular orientations of the methyl groups of the two isomers.

The most stable  $(BA)_2^-$  structure, shown in Figure 5 (left), consists of one BA moiety (front BA in top view and top BA in side view) adopting the an structural motif and the other—the nu structural motif, as defined in Figure 4. As seen in the side view in Figure 5, due to the intermolecular interactions in the dimer anion, each of the BA moieties is slightly distorted from their unsolvated  $C_{2h}$  symmetry geometries. In particular, the heavy atoms of each of the BA moieties within the dimer no longer lie in one plane. However, the qualitative an or nu character of each monomer moiety, as defined by the torsional orientation of the methyl groups, is preserved in the cluster environment. The overall structure belongs to the  $C_2$  symmetry point group and will be referred to as C2 (an-nu). This structure is chiral: taking its mirror image in the plane between the two monomer groups results in a  $C_2$  (nu-an) structure that cannot be superimposed with the original  $C_2$  (an-nu). The other two, less stable structures in Figure 5 are each of  $D_2$ symmetry. In each of them, both BA moieties adopt the same structural motif: an in one case and nu in the other, with the  $D_2$ (an-an) structure being slightly more stable than  $D_2$  (nu-nu).

It may seem logical that the most stable dimer anion structure,  $C_2$  (an-nu), would be described as an ion—molecule complex, BA $^{-}$ BA, with the dot indicating a noncovalent (electrostatic) interaction between the anion "solute" and the neutral "solvent". However, as discussed in Section 3.2, such interaction is inconsistent with the large (larger than in BA $^{-}$ ·H<sub>2</sub>O) band shift in the (BA)<sub>2</sub> $^{-}$  experimental data relative to BA $^{-}$ . An ion-neutral BA $^{-}$ ·BA structure is also not what is indicated by the calculations.

The  $C_2$  (an-nu) description of the geometric structure of  $(BA)_2^-$  does not imply that the an BA moiety is the BA<sup>-</sup> anion solvated by the second, neutral BA (nu). Both in the anion and in the ground singlet state of unsolvated BA, the nu and an geometries are very close in energy:  $\Delta E_{an-nu} = 0.028$  eV and -0.086 eV, respectively (see Section 4.1). Such small energy gaps will not prevent electron delocalization between the an and nu BA moieties in the dimer anion. In comparison, the intermolecular interactions in  $(BA)_2^-$  result in a band shift that is an order-of-magnitude greater than the above  $\Delta E_{an-nu}$  values. Interactions of such magnitude may change the relative

stability of the *an* and *nu* geometries, and, therefore, no correlation between the *an* and *nu* structural motifs and the charge of the corresponding BA moiety within a cluster can be assumed. Supporting this point, the Mulliken charges of the *an* and *nu* moieties in the  $C_2$  (*an-nu*) structure are -0.52 and -0.48, respectively. The delocalized, nearly even charge distribution between the two monomers suggests covalent interaction, likely involving  $\pi-\pi$  bonding between the two BA moieties. Moreover, the  $C_2$  (*an-nu*) structure of  $(BA)_2^-$  is only slightly more stable than the other two dimer anion structures shown in Figure 5,  $D_2$  (*an-an*) and  $D_2$  (*nu-nu*). For the latter two structures, symmetry requires that the excess charge is equally shared between the two monomer groups.

We also used DFT to investigate the trimer anion,  $(BA)_3^-$ . Similar to the experimental motivation, discussed in Section 3.2, the rationale for this part of theoretical work was to determine the structural characteristics of  $(BA)_n^-$  clusters larger than the dimer. The specific question about the intermolecular interactions in these clusters is whether they include a dimer-anion,  $(BA)_2^-$ , as a cluster core, with the additional BA moieties playing the role of neutral solvent. The neutral solvent molecules would be bound to the cluster core by means of relatively weak noncovalent interactions. In this scenario, a significantly smaller band shift from n=2 to n=3 would be expected, compared to the shift observed for the dimer compared to the monomer. Theory should then also identify the presence of (nearly) neutral "solvent" moieties within the calculated cluster structures.

For  $(BA)_3^-$ , the configuration (geometry) space is much vaster than for  $(BA)_2^-$ . For this reason, exploratory calculations starting from various initial trimer geometries were not attempted. Instead, we hypothesized that a plausible (BA)<sub>3</sub> structure could be based on the most stable structural motif of the dimer anion. In the proposed trimer structure, a third BA moiety adopting the nu structural motif is added to the  $C_2$  (annu) dimer-anion structure shown in Figure 5, so that the resulting trimer has a triple-decker appearance, with the an moiety (expected to carry the largest fraction of the negative charge) "sandwiched" in between the two nu moieties: nu-annu. Similar to the dimer anion structures, the proposed trimer structure is well suited to benefit from  $\pi$ – $\pi$  bonding between the monomers. The resulting overall structure is of  $C_{2h}$ symmetry; it was optimized using the M06-2X method, and the result is shown in Figure 6. The complete coordinates are in the Supporting Information.

The distributions of the combined Mulliken charges between the top (nu), middle (an), and bottom (nu) BA moieties in this structure are -0.285, -0.43, and -0.285. As expected, the middle (an) moiety carries the largest charge, maximizing the overall intermolecular interactions within the cluster. Since the charge in the trimer is distributed among three monomer groups, the individual interactions within each an-nu pair are expected to be weaker than in the  $C_2$  (an-nu) dimer-anion. This is reflected in the greater separation between the BA moieties in the trimer compared to the dimer: 3.41 Å (Figure 6) vs 2.98 Å (Figure 5, left). The monomer separation in each case is defined as the distance between the centers of the respective C2–C3 bonds (see Figure 4 for atom numbers).

Similar to the dimer anion, the  $(BA)_3^-$  structure is bound primarily by means of  $\pi - \pi$  interactions between the BA moieties. To illustrate the  $\pi - \pi$  bonding in the dimer and the trimer, Figure 7 shows the highest/singly occupied molecular orbitals (HOMO) of the following: (a) the monomer, (b) the

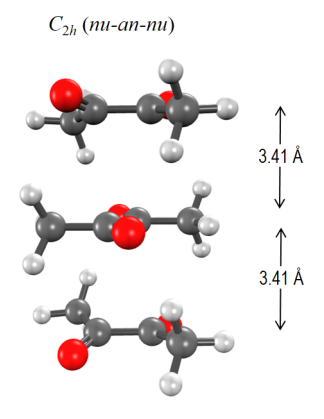


**Figure 6.** A plausible  $(BA)_3^-$  structure optimized at the M06-2X level of theory with the aug-cc-pVDZ basis set. The structure is of  $C_{2h}$  symmetry and adopts a *nu-an-nu* structural motif. The complete structure with all coordinates is included in the Supporting Information. The distribution of the Mulliken charges between the top-middle-bottom BA moieties in this structure is -0.285, -0.43, -0.285. The distance between the middle and top/bottom monomer moieties, defined the same way as in Figure 5, is 3.41 Å. The energy of this structure (defined as the negative of the solvation energy) is -1.670 eV, i.e., it is 1.670 eV more stable than the  $2BA + BA^-$  dissociation limit (see Table 2).

dimer, and (c) the trimer anions of biacetyl. The orbital plots are from the M06-2X calculations and correspond to the BA<sup>-</sup>, (BA)<sub>2</sub><sup>-</sup>, and (BA)<sub>3</sub><sup>-</sup> structures shown in Figures 4 (bottom), 5 (left), and 6, respectively (the perspectives were adjusted to facilitate the comparison of the orbitals).

The BA<sup>-</sup> HOMO, shown in Figure 7(a), has a  $\pi$  bonding character along the central C–C bond and a  $\pi^*$  antibonding character along the two carbonyl groups. Since this MO is singly occupied in the anion, but vacant in the neutral, the above  $\pi$  and  $\pi^*$  properties explain the shortening of the C–C bond and the elongation of the C=O bonds in the anion relative to neutral BA. Moreover, these features of the BA<sup>-</sup> HOMO are similar to those in glyoxal<sup>5</sup> and methylglyoxal.<sup>6</sup>

Figure 7(b) indicates that excess electron in the dimer anion occupies an *inter*molecular orbital resulting from a bonding

overlap of the C–C  $\pi$  lobes of the monomer orbitals. Again, the orbital shown in Figure 7(b) is vacant in the neutral but (singly) occupied in the dimer anion. Therefore, the interaction between the two BA moieties in  $(BA)_2^-$  can be described as an order-of-1/2  $\pi$ – $\pi$  covalent bond. Similarly, the trimer-anion HOMO in Figure 7(c) indicates  $\pi$ – $\pi$  bonding between the terminal BA moieties and the central BA in the *nu-an-nu*  $(BA)_3^-$  structure. Since this MO is singly occupied and delocalized between two intermolecular bonds, each of the *nu-an* bonds in  $(BA)_3^-$  has a bond order of 1/4.

4.4. Solvation Energetics in Biacetyl Cluster Anions. We now discuss the energetics of the various  $(BA)_n^-$  species and establish their relationship to the experimentally observed photoelectron bands and band shifts. Table 2 summarizes three types of energetic parameters for  $(BA)_n^-$  cluster anions: (1) the experimental VDEs and the corresponding band shifts ( $\Delta VDE$ ), defined either relative to BA or relative to the preceding member of the series, i.e., sequential; (2) the calculated VDEs for BA<sup>-</sup>, (BA)<sub>2</sub><sup>-</sup>, and (BA)<sub>3</sub><sup>-</sup> (from these VDEs, the corresponding  $\Delta$ VDE are also calculated); (3) the "solvation" energies  $E_{\text{soly}}(n)$ , defined as the adiabatic difference between the isolated monomer building blocks and the cluster. All VDEs discussed in this Section correspond to transitions to the lowest neutral singlet state (band A in Figure 1). In all calculations for the dimer and trimer anions, the respective  $C_2$ (an-nu) and  $C_{2h}$  (nu-an-nu) structures from Figures 5 and 6 were assumed.

First, we note that the VDEs calculated using the M06-2X functional, VDE (DFT) in Table 2, do not agree particularly well with the experimental values for any of the species studied. However, the shifts (deltas) of the cluster anion VDEs relative to BA $^-$ ,  $\Delta$ VDE (DFT), are in much better agreement with the experimental band shifts. This is not surprising, since the M06-2X functional is designed to perform well for intermolecular interactions,  $^{29}$  reflected in  $\Delta$ VDEs.

When it comes to the *intra*molecular electronic structure and hence the VDE of BA<sup>-</sup>, the CCSD method is by far superior to DFT. This prompted us to construct composite theoretical predictions for the VDEs of  $(BA)_n^-$ , n = 1-3. The composite VDEs are calculated by adding the  $\Delta$ VDE (DFT)

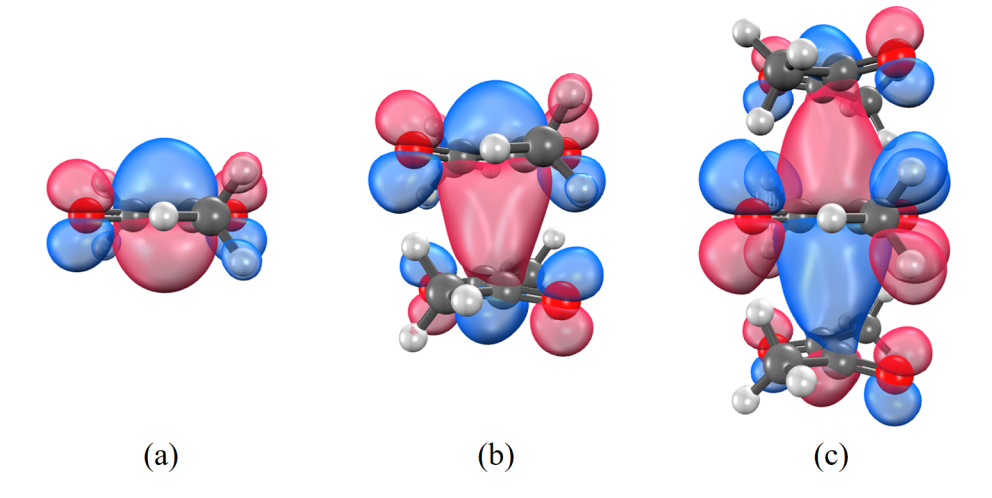


Figure 7. Highest occupied molecular orbitals of (a) BA<sup>-</sup> (the *an* structure shown in Figure 4, bottom), (b)  $(BA)_2^-$  (the *an-nu* structure shown in Figure 5, left), and (c)  $(BA)_3^-$  (the *nu-an-nu* structure shown in Figure 6). Different perspectives (viewpoints) have been chosen in this figure, compared to the above figures. The orbital plots are from the M06-2X/aug-cc-pVDZ calculations and correspond to the isosurface values of (a) 0.10, (b) 0.08, and (c) 0.05. The MOs shown are singly occupied in the respective anions and responsible for the  $\pi-\pi$  covalent bonding between the individual BA moieties in the dimer and trimer anions.

values for the given cluster relative to the monomer anion, calculated using the M06-2X method (given in Table 2), to the CCSD value of the VDE of BA $^-$  (1.092 eV from Table 1). In this approach, both the *intra*- and *inter*molecular interactions in (BA) $_n^-$  are described by methods that perform reasonably well for the task at hand. The resulting VDE (CCSD+DFT) predictions are given in Table 2, in comparison with the experimental results. The agreement is quite good for all species studied.

We note in particular the very good agreement of  $\Delta VDE$ (DFT) for the dimer relative to the monomer, 0.569 eV, with the corresponding experimental band shift, 0.59(1) eV (Table 2). This agreement lends confidence to the proposed dimer and also encourages us to consider the VDE increase for  $(BA)_3$  relative to  $(BA)_2$ . In Table 2, the dimer to trimer VDE increase is nearly the same as that for the monomer to dimer: 0.565 eV vs 0.569 eV. That is, the proposed trimer anion structure is characterized by an equally strong bonding of the third BA moiety to the cluster as of the second. This is because the proposed trimer structure features distributed charge and bonding; it truly is a trimer anion, rather than an ion-molecule complex of the (BA)<sub>2</sub> cluster core and a BA solvent "molecule". However, the experimental dimer-to-trimer band shift is somewhat smaller than the theory prediction: 0.45(1) eV vs 0.565 eV. It is still as large as that for BA-H<sub>2</sub>O relative to BA<sup>-</sup> but smaller than expected for the proposed  $C_{2h}$ (nu-an-nu) trimer structure nonetheless. We can only speculate that the true trimer structure is probably a combination of the distributed-charge character predicted by DFT and a somewhat weaker bonded ion-molecule complex.

Finally, we turn to "solvation" energies  $E_{\text{solv}}(n)$ , calculated for the dimer and trimer anion. The term solvation is in quotation marks, because the so-called solvation interactions in  $(BA)_n^-$  involve a significant degree of covalent character.  $E_{\text{soly}}(n)$  is defined as the adiabatic energy difference between the sum of the isolated neutral and anion monomer groups, on the one hand, and the cluster anion, on the other:  $E_{\text{solv}}(n) =$  $[E(BA^-) + (n-1)E(BA)] - E((BA)_n^-)$ . Thus,  $E_{soly}(n)$  is the total energy involved in assembling the cluster from its asymptotic building blocks. It is a combination of intermolecular (e.g., solvation) and intramolecular (internal perturbations of the solute and the solvent) effects. In photoelectron spectroscopy of cluster anions, the experimental band shifts are often interpreted as the solvation energy of the cluster.<sup>30</sup> This interpretation assumes that the interactions between the neutral species in the final state are negligible and that the intermolecular interactions within the cluster do not significantly perturb the internal structures of the constituents. These assumptions do not apply to (BA), -. As a result, in Table 2 we observe large discrepancies (~0.4 eV for the dimer and ~0.5-0.6 eV for the trimer) between the calculated  $E_{\text{soly}}(n)$  values, on the one hand, and both the  $\Delta \text{VDE}$  (DFT) and the experimental band shifts, on the other.

To analyze this effect, we consider the energy diagram in Figure 8, which illustrates the formation of  $(BA)_2^-$  from the  $BA^- + BA$  and the corresponding photodetachment processes. The diagram is constructed using the M06-2X results, but the qualitative conclusions would remain unchanged if any reasonable computational method were used. The asterisks indicate excited neutral species formed in vertical photodetachment of the corresponding anions. It is clear based on the diagram that the VDE shift underestimates the magnitude of the interactions involved in the formation of the dimer

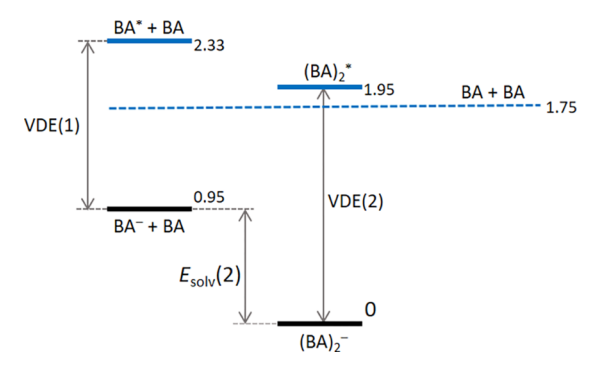


**Figure 8.** Energy diagram for the formation and photodetachment of the  $(BA)_2^-$  cluster anion. The electronic energy values calculated using the M06-2X/aug-cc-pVDZ method are given in eV relative to  $(BA)_2^-$ . The diagram shows that the VDE increase from n=1 to n=2 in the  $(BA)_n^-$  series,  $\Delta \text{VDE}(2) = \text{VDE}(2) - \text{VDE}(1)$ , cannot be used as an accurate estimate of  $E_{\text{soly}}(2)$ .

anion. This is primarily due to the intermolecular interactions in the dimer significantly perturbing the structure (and hence the energy) of the excited  $(BA)_2^*$  dimer species, initially formed in the photodetachment, relative to  $BA^* + BA$ .

### 5. CONCLUSIONS

We have reported photoelectron spectra of biacetyl and its cluster anions. Similar to previously studied methylglyoxal, biacetyl is characterized by distinct torsional angles of the methyl groups relative to the molecule in the neutral singlet state, on the one hand, and the anion and triplet states, on the other. In addition, there are other significant geometric differences between the anion and the neutral singlet state, while the triplet geometry is overall more similar to that of the anion. Accordingly, the BA<sup>-</sup> photoelectron spectra feature a broad and congested singlet band and a narrower and less congested triplet transition. The experimentally determined electron detachment energies are in agreement with ab initio predictions, giving confidence to the theoretically determined anion and neutral structures.

Investigation of biacetyl cluster anions revealed that the intermolecular interactions in the homogeneously solvated clusters  $(BA)_n^-$  are stronger than in the heterogeneous clusters  $BA^-\cdot N_2O$  and  $BA^-\cdot H_2O$ . To account for these observations,  $\pi^-\pi$  bonded structures of the dimer and trimer anions are proposed. Their analysis indicates that the excess charge in the  $(BA)_n^-$  cluster anions (at least the dimer and the trimer) is significantly delocalized between all BA moieties present, and there is a significant degree of covalent  $(\pi^-\pi)$  bonding within the cluster.

#### ASSOCIATED CONTENT

# S Supporting Information

The Supporting Information is available free of charge on the ACS Publications website at DOI: 10.1021/acs.jpca.9b01302.

Complete Cartesian and Z-matrix coordinates of the calculated  $(BA)_2^-$  and  $(BA)_3^-$  cluster anion structures reported in Figures 5 and 6, respectively (PDF)

# AUTHOR INFORMATION

# **Corresponding Author**

\*E-mail: sanov@u.arizona.edu.

#### ORCID ®

Andrei Sanov: 0000-0002-2373-4387

#### Notes

The authors declare no competing financial interest.

#### ACKNOWLEDGMENTS

The authors gratefully acknowledge the support of this work by the U.S. National Science Foundation through Grant CHE-1664732.

#### REFERENCES

- (1) Rossignol, S.; Aregahegn, K. Z.; Tinel, L.; Fine, L.; Noziere, B.; George, C. Glyoxal Induced Atmospheric Photosensitized Chemistry Leading to Organic Aerosol Growth. *Environ. Sci. Technol.* **2014**, *48*, 3218–3227
- (2) Pan, S. S.; Wang, L. M. The Atmospheric Oxidation Mechanism of O-Xylene Initiated by Hydroxyl Radicals. *Acta Physico-Chimica Sinica* **2015**, *31*, 2259–2268.
- (3) Zhang, G.; Mu, Y. J.; Zhou, L. X.; Zhang, C. L.; Zhang, Y. Y.; Liu, J. F.; Fang, S. X.; Yao, B. Summertime Distribution of Peroxyacetyl Nitrate (PAN) and Peroxypropionyl Nitrate (PPN) in Beijing: Understanding the Sources and Major Sink of PAN. *Atmos. Environ.* **2015**, *103*, 289–296.
- (4) Goldstein, A. H.; Galbally, I. E. Known and Unexplored Organic Constituents in the Earth's Atmosphere. *Environ. Sci. Technol.* **2007**, *41*, 1514–1521.
- (5) Xue, T.; Dixon, A. R.; Sanov, A. Anion Photoelectron Imaging Spectroscopy of Glyoxal. *Chem. Phys. Lett.* **2016**, *660*, 205–208.
- (6) Dauletyarov, Y.; Dixon, A. R.; Wallace, A. A.; Sanov, A. Electron Affinity and Excited States of Methylglyoxal. J. Chem. Phys. 2017, 147, 013934.
- (7) Kebarle, P.; Chowdhury, S. Electron-Affinities and Electron-Transfer Reactions. *Chem. Rev.* **1987**, 87, 513–534.
- (8) Moulds, L. D. V.; Riley, H. L. The Polymerisation of Methylglyoxal. J. Chem. Soc. 1938, 621–626.
- (9) Ervin, K. M.; Lineberger, W. C., Photoelectron Spectroscopy of Negative Ions. In *Advances in Gas Phase Ion Chemistry*; Adams, N. G., Babcock, L. M., Eds.; JAI Press: Greenwich, 1992; Vol. 1, pp 121–166.
- (10) Chandler, D. W.; Houston, P. L. Two-Dimensional Imaging of State-Selected Photodissociation Products Detected by Multiphoton Ionization. *J. Chem. Phys.* **1987**, *87*, 1445–1447.
- (11) Houston, P. L. Snapshots of Chemistry: Product Imaging of Molecular Reactions. *Acc. Chem. Res.* **1995**, 28, 453–460.
- (12) Heck, A. J. R.; Chandler, D. W. Imaging Techniques for the Study of Chemical Reaction Dynamics. *Annu. Rev. Phys. Chem.* **1995**, 46, 335–372.
- (13) Velarde, L.; Habteyes, T.; Sanov, A. Photodetachment and Photofragmentation Pathways in the  $[(CO_2)_2(H_2O)_M]^-$  Cluster Anions. *J. Chem. Phys.* **2006**, *125*, 114303.
- (14) Wiley, W. C.; McLaren, I. H. Time-of-Flight Mass Spectrometer with Improved Resolution. *Rev. Sci. Instrum.* **1955**, *26*, 1150.
- (15) Johnson, M. A.; Lineberger, W. C. Pulsed Methods for Cluster Ion Spectroscopy. In *Techniques for the Study of Ion Molecule Reactions*; Farrar, J. M., Saunders, W. H., Eds.; Wiley: New York, 1988; pp 591–635.
- (16) Eppink, A. T. J. B.; Parker, D. H. Velocity Map Imaging of Ions and Electrons Using Electrostatic Lenses: Application in Photoelectron and Photofragment Ion Imaging of Molecular Oxygen. *Rev. Sci. Instrum.* 1997, 68, 3477–3484.
- (17) Dribinski, V.; Ossadtchi, A.; Mandelshtam, V. A.; Reisler, H. Reconstruction of Abel-Transformable Images: The Gaussian Basis-Set Expansion Abel Transform Method. *Rev. Sci. Instrum.* **2002**, *73*, 2634–2642.
- (18) Neumark, D. M.; Lykke, K. R.; Andersen, T.; Lineberger, W. C. Laser Photodetachment Measurement of the Electron-Affinity of

- Atomic Oxygen. Phys. Rev. A: At., Mol., Opt. Phys. 1985, 32, 1890–1892.
- (19) Cavanagh, S. J.; Gibson, S. T.; Gale, M. N.; Dedman, C. J.; Roberts, E. H.; Lewis, B. R. High-Resolution Velocity-Map-Imaging Photoelectron Spectroscopy of the O<sup>-</sup> Photodetachment Fine-Structure Transitions. *Phys. Rev. A: At., Mol., Opt. Phys.* **2007**, *76*, 052708.
- (20) Sanov, A.; Nandi, S.; Jordan, K. D.; Lineberger, W. C. Photochemistry of  $(OCS)_n$  Cluster Ions. *J. Chem. Phys.* **1998**, *109*, 1264–1270.
- (21) Habteyes, T.; Sanov, A. Electron Binding Motifs in the  $(CS_2)_n^-$  (n > 4) Cluster Anions. *J. Chem. Phys.* **2008**, *129*, 244309.
- (22) Mabbs, R.; Surber, E.; Velarde, L.; Sanov, A. Effects of Solvation and Core Switching on the Photoelectron Angular Distributions from  $(CO_2)_n^-$  and  $(CO_2)_n^ \bullet$ H<sub>2</sub>O. *J. Chem. Phys.* **2004**, 120, 5148–5154.
- (23) Sherwood, C. R.; Hanold, K. A.; Garner, M. C.; Strong, K. M.; Continetti, R. E. Translational Spectroscopy Studies of the Photodissociation Dynamics of O<sub>4</sub><sup>-</sup>. *J. Chem. Phys.* **1996**, *105*, 10803–10811.
- (24) Hanold, K. A.; Continetti, R. E. Photoelectron-Photofragment Coincidence Studies of the Dissociative Photodetachment of O<sub>4</sub><sup>-</sup>. *Chem. Phys.* **1998**, 239, 493–509.
- (25) Goebbert, D. J.; Sanov, A. Photodetachment, Photofragmentation, and Fragment Autodetachment of  $[O_{2n}(H_2O)_m]^-$  Clusters: Core-Anion Structures and Fragment Energy Partitioning. *J. Chem. Phys.* **2009**, *131*, 104308.
- (26) Khuseynov, D.; Goebbert, D. J.; Sanov, A. Oxygen Cluster Anions Revisited: Solvent-Mediated Dissociation of the Core O<sub>4</sub><sup>-</sup> Anion. *J. Chem. Phys.* **2012**, *136*, 094312.
- (27) Shao, Y. H.; Gan, Z. T.; Epifanovsky, E.; Gilbert, A. T. B.; Wormit, M.; Kussmann, J.; Lange, A. W.; Behn, A.; Deng, J.; Feng, X. T.; et al. Advances in Molecular Quantum Chemistry Contained in the Q-Chem 4 Program Package. *Mol. Phys.* **2015**, *113*, 184–215.
- (28) Krylov, A. I. Equation-of-Motion Coupled-Cluster Methods for Open-Shell and Electronically Excited Species: The Hitchhiker's Guide to Fock Space. *Annu. Rev. Phys. Chem.* **2008**, *59*, 433–462.
- (29) Zhao, Y.; Truhlar, D. G. The M06 Suite of Density Functionals for Main Group Thermochemistry, Thermochemical Kinetics, Noncovalent Interactions, Excited States, and Transition Elements: Two New Functionals and Systematic Testing of Four M06-Class Functionals and 12 Other Functionals. *Theor. Chem. Acc.* 2008, 120, 215–241.
- (30) Castleman, A. W.; Bowen, K. H. Clusters: Structure, Energetics, and Dynamics of Intermediate States of Matter. *J. Phys. Chem.* **1996**, 100, 12911–12944.